



Dual-layer spectral detector CT (SDCT) can improve the detection of mixed ground-glass lung nodules

Zhenghua Zhang¹ · Fang Yin¹ · Shaolei Kang¹ · Xiaoyu Tuo² · Xiaodi Zhang³ · Dan Han¹

Received: 20 September 2022 / Accepted: 16 December 2022 / Published online: 3 January 2023
© The Author(s), under exclusive licence to Springer-Verlag GmbH Germany, part of Springer Nature 2023

Abstract

Background Mixed ground-glass lung nodules are a high-risk factor for lung adenocarcinoma. This study aimed to analyze the value of SDCT electron density imaging in the detection of mixed ground-glass lung nodules (GGNs).

Method 150 patients with GGNs confirmed by chest SDCT and surgical pathology were retrospectively analyzed. GGNs were screened by two senior radiologists by the double-blind method based on conventional CT and SDCT electron density images. Average CT values and electron density (ED) values of GGNs were measured for all, solid and ground-glass.

Result Thirty pGGN cases determined by conventional CT were found to be mGGN on electron density images, including 23 in the invasive adenocarcinoma group (detection rate of 35.38%), which was significantly higher than that of the PGL group (14.89%, $P < 0.05$). In electron density images, average CT values and ED values in the PGL and invasive adenocarcinoma groups with pGGNs were no difference. The average CT value and ED value were significantly higher in the mGGN invasive adenocarcinoma group compared with the PGL group ($P < 0.05$). Meanwhile, ROC curve analysis of average CT value and ED value revealed AUC values for mGGN infiltration of 0.759 and 0.752.

Conclusion SDCT can improve GGN visualization and increase the detection rate of mGGN compared with conventional CT. Attention should be paid to invasive adenocarcinoma for lung GGNs detected as mGGNs with high average CT value or ED value.

Keywords Lung cancer · Pulmonary nodule · Adenocarcinoma · Computed tomography

Introduction

With the wide application of low-dose chest CT (LDCT) screening, the detection rate of early lung cancer has increased significantly (Kim Yeon et al. 2021), and the CT manifestations of early lung cancer are often ground-glass nodules (GGNs). GGNs can be divided into pure (pGGNs) and mixed (mGGNs) GGNs according to whether there are solid components in GGNs. Although a GGN is a non-characteristic manifestation of lung lesion, persistent GGNs increase the odds of malignancy (especially mGGNs)

(Mazzone Peter and Lam 2022). In 2021, the WHO classified atypical adenomatous hyperplasia (AAH) and adenocarcinoma in situ (AIS) as precursor glandular lesion (PGL) in the new classification of lung tumors. Invasive adenocarcinomas include minimally invasive adenocarcinoma (MIA) and invasive adenocarcinoma (ICA) (WHO Classification of Tumours Editorial Board 2021). In lung adenocarcinoma with GGNs, the degree of invasion of mGGNs is higher than that of pGGNs (Peng et al. 2021). Therefore, early identification of mGGNs is particularly important. Dual-layer Spectral Detector CT (SDCT) is the latest detector-based energy spectrum CT method, which can enable imaging with more parameters such as single energy, iodine density and electron density imaging. Among them, electron density imaging can generate electron density-based images that cannot be generated by conventional CT. This provides a new way for clinical workers to explore the process of disease diagnosis. Recent studies have found that the electronic cloud density map of SDCT can effectively improve the detection of early ground-glass exudate lesion in the lungs of COVID-19

✉ Dan Han
kmhandan@sina.com

¹ Medical Imaging Department, First Affiliated Hospital of Kunming Medical University, Kunming, China

² Pathology Department, First Affiliated Hospital of Kunming Medical University, Kunming, China

³ Philips Healthcare, Chengdu, China

patients (Daoud et al. 2021). The purpose of this study was to evaluate the detection of GGNs in the lung by SDCT-based electronic cloud density images and to compare PGL and invasive adenocarcinoma.

Materials and methods

Patients

A total of 150 patients with lung GGNs confirmed by plain chest SDCT scan and surgical pathology from May 2021 to September 2021 were enrolled, including 62 males and 88 females, aged 25–70 years with an average of 48 ± 11 years. Postoperative pathology confirmed 57 cases in the PGL group (12 AAH and 45 AIS cases) and 93 in the invasive adenocarcinoma group (72 MIA and 21 ICA cases). Inclusion criteria were: (1) GGNs detected by SDCT, pathologically confirmed (gold standard) and untreated; (2) GGN diameter ≤ 3 cm in the lung window. Exclusion criteria were: (1) other lung tumors; (2) poor image quality. All patients were informed and signed informed consent.

CT examinations

Chest scans were performed on dual-layer spectral detector CT (IQon Spectral CT, Philips Healthcare). All patients were scanned in the supine position, head first. To ensure that all lung tissues were covered, scans were performed from the thoracic inlet to the costophrenic. Scanning parameters: tube voltage 120 kV, automatic tube current modulation, rotation speed 0.33 s/rot; helical pitch 0.938, detector collimation 64×0.625 mm, image reconstruction matrix 512×512 , layer thickness 1 mm, layer spacing 0.7 mm. Patients were scanned only once, and both conventional CT images and Spectral Base Images (SBI) were obtained. Lung window (window width: 1500HU, window position: -400 HU) was used for image analysis.

Image analysis

GGNs were screened by two senior radiologists with more than 5 years of work experience using the double-blind method based on conventional CT images. In case of disagreement, a third senior radiologist was invited to review the data for a consensual discussion. Spectral Base Images (SBI) data were transferred to the post-processing workstation to reconstruct electron density images. GGNs were screened by the same 2 senior radiologists according to electron density images. The average CT and electron cloud density values of all, solid and ground-glass GGNs were measured, respectively, and the region of interest (ROI) was taken as the 3D volume (avoiding blood vessels and the bronchus).

For GGNs, hyperdense shadows in the lung were well or poorly defined but not dense enough to mask the moving vessels and the bronchus. PGGNs and mGGNs are GGNs with and without solid components, respectively (Xiaoju et al. 2018). The Electron Density value (ED) displays the relative value distribution diagram of the electron density corresponding to each voxel, i.e., the ratio of electron density to that of water, expressed in (%EDW).

Statistical analysis

The SPSS 26.0 software was used for data processing. Count data were presented as number (n), and measurement data with normal distribution as $\bar{x} \pm S$. The groups were compared by the four-grid Chi-square test and one-way ANOVA. Receiver Operator characteristic (ROC) curve analysis was performed to assess the diagnostic efficiency of average CT value and ED. $P < 0.05$ was considered statistically significant.

Results

Lung GGN detection by conventional CT and SDCT

Based on conventional CT, 112 pGGN cases were screened by 2 senior physicians, including 47 in the PGL group (10 AAH and 37 AIS cases) and 65 in the invasive adenocarcinoma group (52 MIA and 13 ICA cases). There were 38 mGGN cases, including 10 in the PGL group (2 AAH and 8 AIS cases) and 28 in the invasive adenocarcinoma group (20 MIA and 8 ICA cases). The same two senior physicians assessed the cases based on the electronic cloud density map, and found that 30 PGGNs were mGGNs, with a 20.00% increase compared with conventional CT. According to electron density imaging, 82 pGGNs were screened, including 40 in the PGL group (10 AAH and 30 AIS cases) and 42 in the invasive adenocarcinoma group (32 MIA and 10 ICA cases). There were 68 mGGNs, including 17 in the PGL group (2 AAH and 15 AIS cases) and 51 in the invasive adenocarcinoma group (40 MIA and 11 ICA cases), as shown in Table 1. According to electron density images, among 112 pGGN cases, 23 mGGNs (detection rate of 35.38%) were detected in the invasive adenocarcinoma group, and 7 (detection rate of 14.89%) in the PGL group. The difference in detection rates between the two groups was statistically significant ($\chi^2 = 5.840$, $P = 0.016$).

Average CT and ED values

In the 30 new mGGN cases, average CT values for the solid and ground-glass parts were -500.87 ± 124.42 HU and -696.07 ± 77.40 HU, respectively, and average ED

Table 1 GGNs detected by conventional CT and electron density imaging

	Conventional CT image		Electron density image	
	PGL	Invasive adenocarcinoma	PGL	Invasive adenocarcinoma
pGGN	47	65	40	42
mGGN	10	28	17	51
Total	57	93	57	93

GGNs ground-glass lung nodules, pGGN pure ground-glass lung nodule, mGGN mixed ground-glass lung nodule, PGL precursor glandular lesion

values were $45.80 \pm 11.90\%$ and $30.01 \pm 7.80\%$, respectively. The differences were statistically significant ($T = -7.296$ and $T = -6.077$, respectively; both

$P = 0.000$), as shown in Figs. 1, 2. On electron density images, the average CT values of the PGL and invasive adenocarcinoma groups with pGGN were -651.18 ± 82.62 HU and -665.59 ± 81.01 HU, respectively, and average ED values were $33.11 \pm 8.44\%$ and $30.98 \pm 7.56\%$, respectively. The differences were not statistically significant ($T = 0.797$, $P = 0.428$ and $T = 1.196$, $P = 0.235$, respectively), as shown in Fig. 3. On electron density images, average CT values for the PGL and invasive adenocarcinoma groups with mGGNs -643.74 ± 61.66 HU and -555.39 ± 95.37 HU, respectively, while average ED values were $33.79 \pm 5.50\%$ and $43.05 \pm 10.29\%$, respectively. The differences were statistically significant ($T = 3.569$ and $T = 3.531$, respectively; both $P = 0.001$). At the same time, ROC curve analysis was performed for average CT and ED values, and AUCs for identifying mGGN infiltration were 0.759 and 0.752, respectively, as shown in Fig. 4.

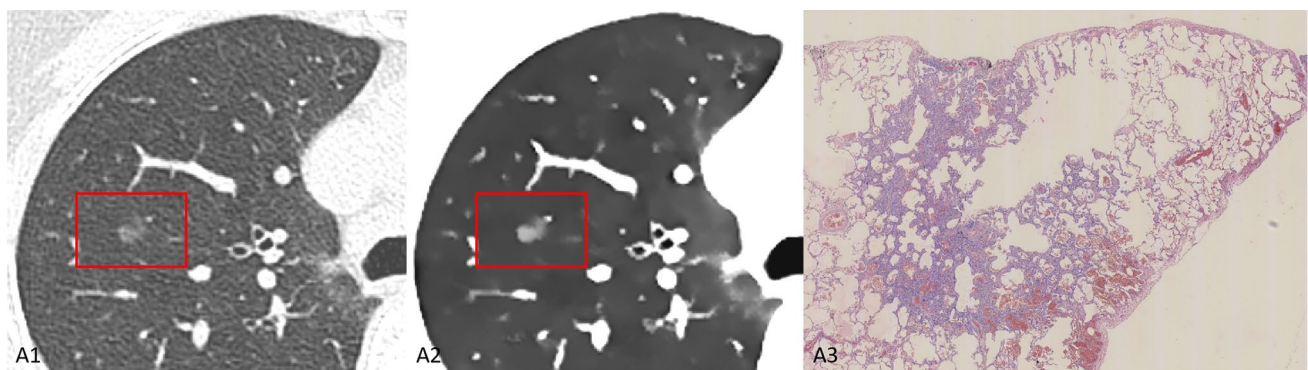


Fig. 1 A1 Conventional CT image, with a nodule in the anterior segment of the upper lobe of the right lung showing a pGGN (red box). A2 Electron density image, with a nodule in the anterior segment of

the upper lobe of the right lung being a mGGN (red box); A3 Pathologic map (1.5x, H&E staining) of a MIA, with unclear local boundary of the tumor and ununiform distribution

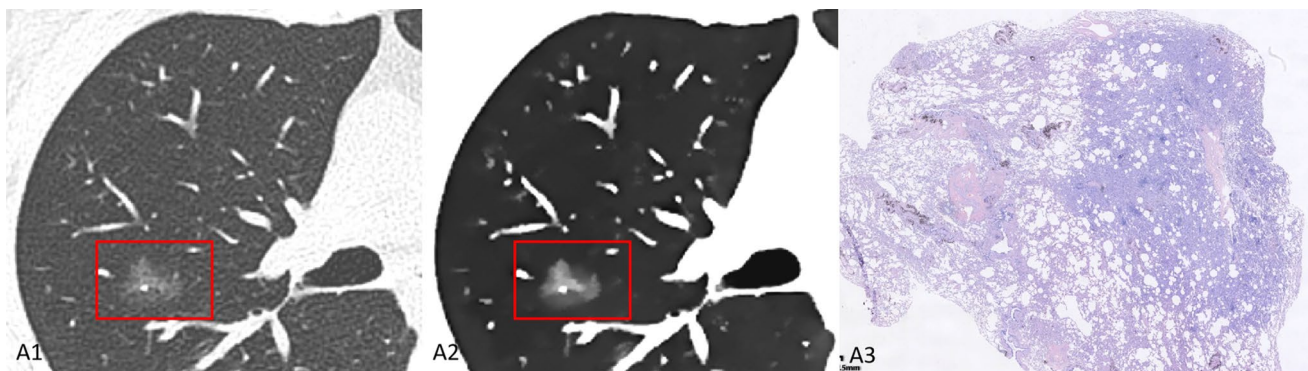


Fig. 2 A1 Conventional CT image, with a nodule in the posterior segment of the upper lobe of the right lung showing a pGGN (red box). A2 Electron density image, with a nodule in the posterior segment of

the upper lobe of the right lung being a mGGN (red box). A3 Pathologic map (1.5x, H&E staining) of an ICA, with unclear boundary of the tumor, ununiform distribution and local collapse of the air cavity

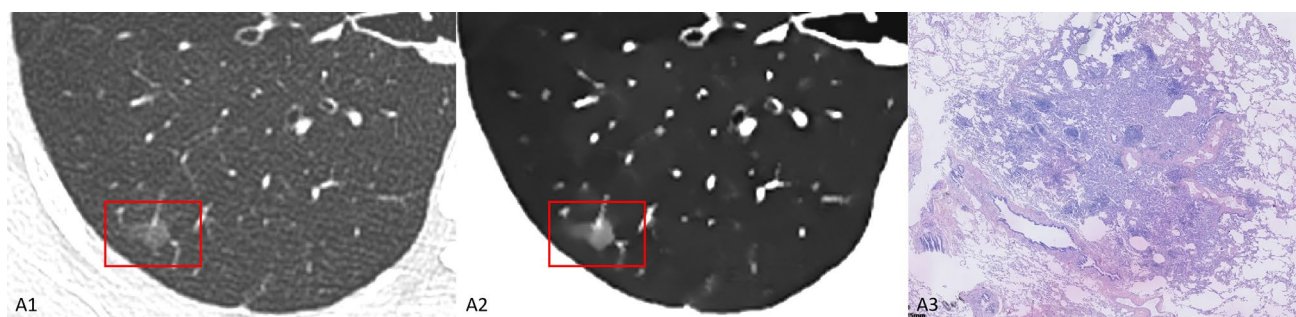


Fig. 3 **A1** Conventional CT image, with a nodule in the dorsal segment of the lower lobe of the right lung showing a pGGN (red box). **A2** In the electron density image, a nodule in the dorsal segment of

the lower lobe of the right lung still showing a pGGN (red box). **A3** Pathologic map (1.5x, H&E staining) of an AIS, tumor with clear boundary and uniform distribution

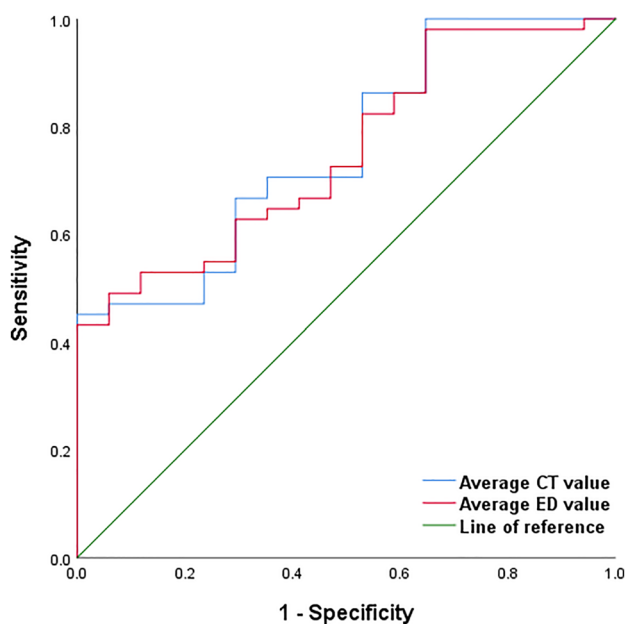


Fig. 4 On electron density images, ROC curve analysis of average CT and ED values in the PGL and invasive adenocarcinoma groups (mGGNs)

Discussion

At present, lung cancer is one of the tumors with a high incidence worldwide, and its mortality still ranks first (Sung et al. 2021). The clinicopathological characteristics of lung adenocarcinoma with GGNs are different from those of pure lung adenocarcinoma, and GGNs have become a special clinical subtype (Ye et al. 2019). According to lung-RADS (Pulmonary Imaging Reporting and Data System), aggressive treatment of mGGNs is more cost-effective than pGGNs (Hammer Mark et al. 2021). Therefore, how to accurately evaluate the characteristics of pulmonary nodules and provide a strong reference

for clinical diagnosis and treatment strategies has become an urgent need. In recent years, with the development of the computer technology, a series of auxiliary diagnostic systems for pulmonary nodules have emerged. Studies have pointed out that the use of pulmonary nodular auxiliary diagnostic systems can effectively describe the characteristics of GGNs, determine GGN aggressiveness before surgery, and help clinicians develop personalized treatment strategies (Hui et al. 2022; Li et al. 2022a). However, the application of these auxiliary diagnostic systems in clinic is limited and the standards are inconsistent, and clinicians cannot intuitively observe pulmonary nodules. This study attempted to observe the characteristics of lung GGNs using electron density imaging of SDCT, to increase the detection rate of lung mGGNs and compare PGL and invasive adenocarcinoma cases.

Influence of solid components of lung GGNs on pathological classification

In this study, electron density imaging detected 30 more mGGN cases than conventional CT, with a 20.00% increase in the detection rate. Conventional CT cannot directly reveal electron density, which usually needs to be obtained by CT value conversion. However, SDCT can yield electron density directly through a conventional scan without CT value conversion, and results are more accurate than those of conventional CT. On electron density images, the average CT and ED values of the relatively real part of mGGNs are higher than those of the ground-glass part, suggesting that the internal density of pGGN detected by conventional CT is uneven, which is shown as mGGNs on electron density images. Compared with lung cancer with solid nodules, lung cancer with GGNs is characterized by inhibited metabolism and inactive immune microenvironment, which may be the mechanism of its clinically inert progression (Chen et al. 2021). The amounts of solid components in lung GGNs are highly correlated with the degree of pathological invasion.

When a GGN contains solid components, the probability of adenocarcinoma is as high as 90% (Hattori et al. 2021; Ma et al. 2021). This study found that among 30 mGGN cases, the detection rate was significantly higher in the invasive adenocarcinoma group compared with the PGL group (35.38% vs 14.89%), indicating that mGGNs are more likely to progress to adenocarcinoma. According to previous findings, GGNs with clear boundary, lobulated shape and scattered irregular solid components are prone to vicious transformation (Li et al. 2022b). Some GGNs in this study showed irregular solid components on electron density images, which was confirmed by postoperative pathology as invasive adenocarcinoma (Fig. 3). Scholars have pointed out that using artificial intelligence to analyze the image characteristics of solid components and ground-glass components in GGNs would help diagnose the invasiveness of lung adenocarcinoma, and show better predictive performance than the conventional gross tumor model (Wu et al. 2020). At the same time, Li Yanmeng et al. found that a higher proportion of solid components in GGNs are accompanied by higher mutation frequencies in EGFR, TP53, RBM10 and ARID1B through radiogenomic analysis, indicating that these genes play roles in the progression of lung cancer (Li et al. 2020). Ding Hongdou et al. pointed out that for GGNs larger than 3 cm, the size of the solid component can predict lymph node metastasis and prognosis better than the overall size, and clinical T staging should be based on the size of solid components rather than the overall size of the tumor (Ding et al. 2019). Electron density imaging in this study could detect more mGGNs and clearly display its internal components, which would provide a new approach for subsequent research. Studies suggested that lung GGNs should not be ignored, even if less than 6 mm and stable for 5 years, especially when new solid components occur during follow-up (Lee et al. 2019). For patients with lung GGNs, electron density imaging is expected to detect solid components in the lesion early during follow-up, providing a strong basis for early clinical intervention.

Effects of CT and ED values of lung GGNs on pathological classification

The maximum CT value in lung GGNs may reflect hemorrhage and calcification in nodules, while the minimum CT value reflects the remaining air cavity or bronchus in nodules. Therefore, there may be errors in selecting the maximum or minimum CT value for identification. Whether the measurement of average CT value of lung GGNs can effectively identify the nature of GGNs, most scholars believe that the average CT value of invasive adenocarcinoma is higher than that of PGL, and in case the average CT value increases during follow-up of the nodule, clinical intervention should be carried out (Gao et al. 2020; Tamura et al.

2014). In this study, average CT value in the invasive adenocarcinoma cases with mGGNs was significantly higher than that of the PGL group, corroborating with most studies. However, some scholars believe that the average CT value of lung GGNs cannot distinguish between PGL and invasive adenocarcinoma cases, which may be caused by the difference of collected case samples (different sample contents of pGGNs and mGGNs). Fu Fangqiu et al. found that in pGGN cases, nodular size was the only imaging parameter related to tumor invasion, and the average CT value had no advantage in differentiating pathological types (Fu et al. 2021), which was consistent with the results of this study, which may be related to PGL and MIA, the majority of tumor pathological types presenting pGGN.

As shown above, the mean CT and ED values of SDCT can effectively detect mGGN infiltration (AUCs of 0.759 and 0.752, respectively). The electron cloud density of SDCT is the relative value distribution diagram showing the electron density corresponding to each voxel, and the ED value is the ratio of electron density to water. Recent findings have shown that ED effectively differentiates between benign and malignant GGNs in the differential diagnosis of lung GGNs by plain SDCT images (Qiu et al. 2022), which is consistent with the results of this study.

In conclusion, compared with conventional CT, SDCT can improve GGN visualization, increases the detection rate of mGGNs, and better evaluates the pathological classification of GGNs before surgery. Attention should be paid to invasive adenocarcinoma for lung GGNs detected as mGGNs with high average CT value or ED value. Due to the small sample size included, ICA cases were the least, which may have selection bias and need further investigation.

Author contributions DH contributed the study concept. ZZ designed the study and wrote the main manuscript text. Data acquisition was performed by FY and SK. XT performed pathological analysis. XZ performed statistical analysis. All authors reviewed the manuscript.

Funding This work was supported by Natural Science Foundation of China (No.81960310).

Data availability The datasets generated during and/or analyzed during the current study are available from the corresponding author on reasonable request.

Declarations

Conflict of interest Authors declare that there is no conflict of interest.

Informed consent All participants were signed the informed consent.

References

- Chen K, Bai J, Reuben A et al (2021) Multiomics analysis reveals distinct immunogenomic features of lung cancer with ground-glass opacity. *Am J Respir Crit Care Med* 204(10):1180–1192
- Daoud B, Cazejust J, Tavolaro S et al (2021) Could spectral CT have a potential benefit in coronavirus disease (COVID-19)? *Am J Roentgenol* 216(2):349–354
- Ding H, Wang H, Zhang P et al (2019) Prognostic factors of lung adenocarcinoma manifesting as ground glass nodules larger than 3cm. *Eur J Cardiothorac Surg* 55(6):1130–1135
- Fu F, Zhang Y, Wang S et al (2021) Computed tomography density is not associated with pathological tumor invasion for pure ground-glass nodules. *J Thorac Cardiovasc Surg* 162(2):451–459
- Gao C, Li J, Wu L et al (2020) The natural growth of subsolid nodules predicted by quantitative initial CT features: a systematic review. *Front Oncol* 10:318
- Hammer Mark M, Eckel Andrew L, Palazzo Lauren L et al (2021) Cost-effectiveness of treatment thresholds for subsolid pulmonary nodules in CT lung cancer screening. *Radiology* 300(3):586–593
- Hattori A, Suzuki K, Takamochi K et al (2021) Prognostic impact of a ground-glass opacity component in clinical stage IA nonsmall cell lung cancer. *J Thorac Cardiovasc Surg* 161(4):1469–1480
- Hui Z, Hanfei Z, Shan W et al (2022) Invasive prediction of ground glass nodule based on clinical characteristics and radiomics feature. *Front Genet* 12:783391
- Kim Yeon W, Kwon Byoung S, Lim Sung Y et al (2021) Lung cancer probability and clinical outcomes of baseline and new subsolid nodules detected on low-dose CT screening. *Thorax* 76(10):980–988
- Lee HW, Jin KN, Lee JK et al (2019) Long-term follow-up of ground-glass nodules after 5 years of stability. *J Thorac Oncol* 14(8):1370–1377
- Li Y, Li X, Li H et al (2020) Genomic characterisation of pulmonary subsolid nodules: mutational landscape and radiological features. *Eur Respir J* 55(2):1901409
- Li Y, Liu J, Yang X et al (2022a) Prediction of invasive adenocarcinomas manifesting as pure ground-glass nodules based on radiomic signature of low-dose CT in lung cancer screening. *Br J Radiol*. <https://doi.org/10.1259/bjr.20211048>
- Li W-J, Lv F-J, Tan Y-W et al (2022b) Benign and malignant pulmonary part-solid nodules: differentiation via thin-section computed tomography. *Quant Imaging Med Surg* 12(1):699–710
- Ma X, Zhou S, Huang L et al (2021) Assessment of relationships among clinicopathological characteristics, morphological computer tomography features, and tumor cell proliferation in stage I lung adenocarcinoma. *J Thorac Dis* 13(5):2844–2857
- Mazzone Peter J, Lam L (2022) Evaluating the patient with a pulmonary nodule: a review. *JAMA* 327(3):264–273
- Peng M, Yu F, Chen X et al (2021) Comprehensive characterization of genomic and radiologic features reveals distinct driver patterns of RTK/RAS pathway in pulmonary nodules presenting as ground-glass opacity. *J Clin Oncol* 39(15):e20516–e20516
- Qiu J, Xin X, Yang W et al (2022) The value of dual-layer spectral CT single energy image and electron density imaging in differentiating benign and malignant pulmonary ground glass nodules. *Chin J Radiol* 56(2):175–181
- Sung H, Ferlay J, Siegel RL et al (2021) Global cancer statistics 2020: GLOBOCAN estimates of incidence and mortality worldwide for 36 cancers in 185 countries. *CA Cancer J Clin* 71(3):209–249
- Tamura M, Shimizu Y, Yamamoto T et al (2014) Predictive value of one-dimensional mean computed tomography value of ground-glass opacity on high-resolution images for the possibility of future change. *J Thorac Oncol* 9(4):469–472
- WHO Classification of Tumours Editorial Board (2021) WHO classification of tumours. Thoracic tumours. 5th ed. IARC Press, Lyon
- Wu G, Woodruff HC, Shen J et al (2020) Diagnosis of invasive lung adenocarcinoma based on chest CT radiomic features of part-solid pulmonary nodules: a multicenter study. *Radiology* 297(2):451–458
- Xiaoju Z, Li B, Faguang J et al (2018) Chinese expert consensus on the diagnosis and treatment of pulmonary nodules (2018 version). *Chin J Tuberc Respir Dis* 41(10):763–771
- Ye T, Deng L, Wang S et al (2019) Lung adenocarcinomas manifesting as radiological part-solid nodules define a special clinical subtype. *J Thorac Oncol* 14(4):617–627

Publisher's Note Springer Nature remains neutral with regard to jurisdictional claims in published maps and institutional affiliations.

Springer Nature or its licensor (e.g. a society or other partner) holds exclusive rights to this article under a publishing agreement with the author(s) or other rightsholder(s); author self-archiving of the accepted manuscript version of this article is solely governed by the terms of such publishing agreement and applicable law.